Fractal dependence of the packed bed porosity on the particles size distribution

Algis Džiugys [a,*], Amir Houshang Mahmoudi [b], Edgaras Misiulis [a], Robertas Navakas [a], Gediminas Skarbalius [a]

[a] *Laboratory of Heat Equipment Research and Testing, Lithuanian Energy Institute, Breslaujos St. 3, LT-44403 Kaunas, Lithuania*
[b] *Laboratory of Thermal Engineering, University of Twente, P.O. Box 217, 7500AE Enschede, the Netherlands*

ARTICLE INFO

ABSTRACT

Packed beds formed by granular materials are the heart of many engineering and scientific applications. For a better understanding of transport processes occurring in such porous mediums, first the structural characteristics of packed beds should be known. The discrete element method (DEM) has been used widely as a powerful and reliable tool to study packed beds formed by granular materials. In all DEM-based models, the number of particles is a limiting factor as the computational time increases with the number of particles. To overcome this issue, it is common to neglect small particles in the bed. However, due to missed small particles, the porosity of the packed bed is underestimated. This has an impact on the fluid flow and consequently the heat and mass transfer in the bed.

In the present work, a relation between the diameter of the smallest particle in a packed bed and the porosity of the bed is formed by performing a series of well-defined DEM simulations. This relation gives the possibility to consider the effect of small particles on the porosity of the bed without considering them in the computational domain. The results showed that the bed porosity decreases with decreasing the size of the smallest particle. Moreover, it was shown that the relation between the core porosity of the bed and the smallest particle size in the bed can be described by a fractal law.

© 2022 Elsevier Ltd. All rights reserved.

1. Introduction

In many scientific research and engineering applications, porous media in form of granular material is the heart of the system such as drying technology [1], biomass conversion [2], CO_2 capture [3], thermochemical heat storage [4], chemical reactors and geology [5]. In most of these applications, fluid flow or even multiphase flow is extensively used. For a better understanding of transport processes occurring in such porous mediums, first the structural characteristics of packed beds should be known [6]. Nonuniform distribution of the porosity in a randomly packed bed has a significant impact on the flow distribution, pressure drop, heat and mass transfer between fluid and solid phase, especially near the wall region [7–9].

The porosity distribution in a randomly packed bed depends on the packed bed particle size distribution. The Rosin-Rammler size distribution (also called Rosin-Rammler-Sperling-Bennett [10] or Weibull distribution) [11] is one of the most well-known and popular distribution

functions used to describe size distributions of particles generated by fragmentation processes, such as grinding, milling, crushing operations, and also in volcanic and even astronomical applications [12]. Another popular model for describing particle size distribution is the Gates-Gaudin-Schuhmann model, which has been used in the metalliferous mining industry since 1940 due to its simplicity and clarity [13,14]. The Swebrec and Rosin-Rammler models accurately predicted the particle size distributions of metallurgical coke grinding products [15]. To model naturally occurring sediments, the log-hyperbolic and skew log-Laplace size distribution functions were proposed [16,17]. The log-normal distribution (also called Galton's distribution) [10] is often used to model the particle size distribution of aquatic particles, pulverized material, and aerosols.

There are many experimental investigations to get a good insight into the structure of packed beds [5,18–22]. There are different experimental methods to determine the porous structure of a packed bed such as slice-cutting on a lathe [23], using radiography [24], magnetic resonance imaging [25], fluorescence [26] and X-ray tomography [19, 20]. The last method can determine the void space with high resolution however; it requires dedicated and costly equipment. Seckendorff et al. [19] performed a comprehensive X-ray tomography on mono-sized spheres in cylindrical container with tube-to-particle diameter ratios

---

* Corresponding author.
E-mail addresses: algis.dziugys@lei.lt (A. Džiugys), a.mahmoudi@utwente.nl (A.H. Mahmoudi), edgaras.misiulis@lei.lt (E. Misiulis), robertas.navakas@lei.lt (R. Navakas), gediminas.skarbalius@lei.lt (G. Skarbalius).

$\lambda = 3.0$ to 9.0. X-ray tomography has its own limitations such as long scanning time, sample size and low resolution in large samples. Therefore, it cannot be used to study big packed beds, large number of samples and wide range of scales in one sample due to resolution issue (depending on the equipment).

Numerical modelling has been developed significantly in past decades to fill this gap. Discrete element method (DEM) has been used widely as a powerful and reliable tool to study the structure of packed beds [9,27–30]. Combination of Computational fluid dynamic (CFD) with DEM as an advance numerical modelling approach [31,32] offers the opportunity to model multiphase flow through a packed bed and study the heat and mass transfer between different phases with high degree of details [33–35]. This approach has been used in many research and engineering fields such as drying [36], pyrolysis and combustion in the packed bed of biomass [37–39], blast furnace [40,41], pharma industry [42], heat storage [43]. Next to CFD-DEM, there a simplified numerical modelling approach of multi-phase flow through a packed bed (i.e. continuum mechanics [44–46]). Although continuum methods are suitable tools, but is not applicable for all cases or miss accuracy. Continuum mechanics models require particles size distribution, porosity and specific area which should be find experimentally. These are the main drawbacks of continuum methods while in CFD-DEM approach can be addressed easily.

In all DEM based models (i.e. including CFD-DEM), number of particles is a limiting factor as the computational time increases with the number of particles. However, in most of engineering applications we are dealing with packed beds with millions of particles, which is not feasible to consider them in the model. To overcome this issue, it is common to neglect small particles in the bed. This will reduce significantly the total number of particles and consequently the computational time. However, due to missed small particles, porosity of the packed bed is underestimated. This will have impact on fluid flow and consequently heat and mass transfer in the bed.

It would be a great advantage if a model of the bed porosity can offer both reasonable simulation time and high level of accuracy. This is the goal of present study. The main objective of this work is to investigate a possibility to construct a relation between the diameter of the smallest particle in a packed bed and the porosity of the bed. This relation gives the possibility to take into account the effect of small particles on the porosity of the bed without considering them in the computational domain of a CFD-DEM model. This reduces significantly the computational time and consequently brings CFD-DEM models one step further to simulate large scale engineering problems.

2. Method

A number of approaches have been applied for describing dynamics of granular matter with a varying degree of success [38]. The Discrete element method (DEM) proved to be the most accurate, besides, it is simple to implement. In this time-driven method, granular material is regarded as a system of a finite number N of particles with a given shape and visco-elastic material properties. The motions and collisions of each separate particle are tracked using the system of dynamics equations derived from the classical Newtonian mechanics approach based on the Newton's second law for translation and rotation of each particle in the granular material. The angular orientations are ignored for spherical particles.

The equations of motion are integrated, using the 6th–order Gear predictor–corrector scheme [38]. The current state of all particles, all the forces and moments acting on each particle, at the time t, are evaluated and updated after fixed time step Δt, which is much smaller than the smallest time of impacts. Particles are treated as contacting visco-elastic bodies which shapes can overlap each other instead of body deformation. Contact forces depend on the overlap geometry, dynamics parameters and material properties of the particles. Both the tangential and normal components of the repulsion force with visco-elastic models

for energy dissipation and friction are included in the contact forces [30].

The motion of particles is limited by the box made up of flat rectangular walls. Hence, two types of collisions must be treated: between two particles or between a particle and a flat wall. Walls are treated as particles, therefore impacts between walls and particles are resolved by the same force model, only the geometric relations for calculating the normal and tangential force components and the overlap depth need special derivation. All the walls in this model are rectangular and flat with the mass and the radius of wall curvature being infinite. Wall motions are deterministic and wall deformations are not taken into account.

A more detailed description of the DEM model used for this type of numerical simulations, as well as treatment of collisions between spherical particles and flat walls, is presented in [30,38,47].

3. Setup of the numerical experiment

Packing of wood chips approximated by spheres was investigated. The distribution of wood chips size was defined according to [48]. Each mass/volume fraction of wood chips (Fig. 1) was approximated by spherical particles according to volume V_f and number N_f of mean particle in the each fraction, as it is listed in Table 1. Size of the biggest particles was defined as $D_{max} = 18.24$ mm. Number of particles in each fraction was calculated by division of fraction volume by volume of spherical particle representing mean particle in this fraction, while the total volume of all fractions is $8.72 \cdot 10^{-3}$ m^3.

Eight sets of particles have been considered in this work with size range of 0.53 mm $\leq D_f \leq$ 18.24 mm. The largest particle diameter is the same in all sets (i.e. 18.24 mm), while the smallest particle diameter varies in different sets (i.e. from 0.53 mm to 18.24 mm). As an example, the first set is formed by particles from the entire range ($D_f \in [0.53$ mm, 18.24 mm]), while the second set is formed by particles in this range: $D_f \in [1.76$ mm, 18.24 mm]. The last set includes only particles with a diameter of $D_f = D_{max} = 18.24$ mm. Let us note, that the dependency of the cumulative volume of the set of particles fractions on the smallest particles fraction D_{min} included into the set can be approximated as follows (Fig. 1):

$$V_{cum}(D_{min}) = \sum_{D_f=D_{min}}^{D_{max}} V_f(D_f) = \sum_{D_f=D_{min}}^{D_{max}} N_f \frac{4}{3}\pi\left(\frac{D_f}{2}\right)^3 = a_V + b_V \cdot D_{min}$$

(1)
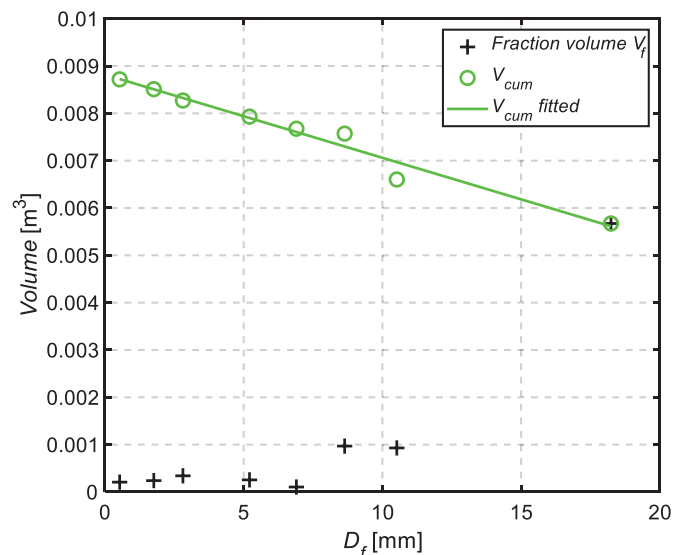
with $a_V = 0.0088173$ and $b_V = -0.17563$.

Fig. 1. Distribution of particles size fraction volume.

Table 1
Distribution of spherical particles of different sizes.

Fraction, [mm]	Fraction volume, V_f, [m³]	Spherical particles diameter, D_f, [mm]	Number of spherical particles in fraction, N_f
$D \geq 10$	$5.672 \cdot 10^{-3}$	18.24	1785
$10 > D \geq 8$	$0.93 \cdot 10^{-3}$	10.52	1526
$8 > D \geq 5$	$0.969 \cdot 10^{-3}$	8.64	2869
$5 > D \geq 4$	$0.104 \cdot 10^{-3}$	6.90	604
$4 > D \geq 3.15$	$0.255 \cdot 10^{-3}$	5.21	3444
$3.15 > D \geq 2$	$0.341 \cdot 10^{-3}$	2.81	29,351
$2 > D \geq 1$	$0.239 \cdot 10^{-3}$	1.76	83,865
$D < 1$	$0.208 \cdot 10^{-3}$	0.53	2,662,294

Packing of spherical particles was numerically simulated in the box of size 0.2 m width in x direction, 0.2 m length in y direction and up to 2 m height in z direction depending on requirements.

The gravity acceleration vector $\vec{g}$ in the laboratory frame of reference is directed downwards along the z axis: $\vec{g} = \{0, 0, -10\}$ m/s². The relevant mechanical properties of the particle material are listed in Table 2.

Case of set particles fractions with $D_{min} = 0.53$ mm ($D < 1$ mm in Table 1) was excluded from simulations due to too big number of particles in the fraction of smallest particles, because a simulation of this case would take enormous computing resources. Therefore only 7 sets of particles fractions with $D_{min} \in \{1.76, 2.81, 5.21, 6.90, 8.64, 10.52, 18.24\}$ mm were simulated.

Hook's contact law was used to describe the normal contact force. The full time of elastic contact for the simulated smallest particles ($D_f = 1.76$ mm) was estimated as $2.1 \cdot 10^{-5}$ s and $1.5 \cdot 10^{-4}$ s for the biggest particles ($D_f = 18.24$ mm), so the time step was choose from $\Delta t = 10^{-7}$ s to $\Delta t = 10^{-6}$ s, depending on the case, in order to ensure that the impact between particles is resolved in more than 20 time steps at least.

The particles packing was obtained by simulating free falling particles under gravity. For this purpose, a rectangular lattice consisting of cubic cells was introduced at the top of the simulation box; the size of each cubic cell was equal to the diameter of the biggest particle. The particles were then placed at the centres of the cells. This setup ensured that the particles did not overlap in their initial configuration. Each particle was assigned a random velocity and allowed to fall freely under the presence of gravity. This process of falling and settling was simulated until the particles come to the rest state. Initial random velocities ensured that the particles assume "random" positions after settling, rather than aligning themselves in a crystal-like pattern, similar to that generated before settling.

It was simulated 38 cases of various particles sizes distributions $[D_{min}, D_{max}]$ for D_{min} varying from 1.76 mm to $D_{max} = 18.24$ mm (Table 1). As it was mentioned above, the smallest fraction with particles size $D < 1$ mm was not included due to limitations of computing resources. The total number of particles in each case varied from $N_p = 2000$ up to $N_p = 60000$ depending on minimal particles

size, and resulting height of the packed bed was from 0.16 m up to 1.51 m.

Fig. 2 shows the visual packing patterns of spheres with different smallest particles size $D_{min} = 1.76$ mm ($N_p = 60000$) and $D_{min} = D_{max} = 18.24$ mm ($N_p = 2000$).

3.1. Final state randomness

In order to estimate the randomness of the final state packing, the size segregation of the particles was estimated by a parameter based on the correlation between the particle position x and the particle size D [30,47]:

$$\vec{S}(t) = \sum_{k=1}^{3} \vec{e}_k \frac{\sum_{i=1}^{N}(D_i - \langle D \rangle)(x_{k,i}(t) - \langle x_k(t) \rangle)}{\sqrt{\sum_{i=1}^{N}(D_i - \langle D \rangle)^2}\sqrt{\sum_{i=1}^{N}(x_{k,i}(t) - \langle x_k(t) \rangle)^2}} \quad (2)$$

where $\vec{e}_k$ is the unit vector of k-th coordinate axis, $x_{k,i}$ is k-th component of the position vector of i-th particle $\vec{x}_i$ ($x_{1,i} \equiv x_i$, $x_{2,i} \equiv y_i$, $x_{3,i} \equiv z_i$), $\langle f \rangle$ is average value of any parameter f of the particle:

$$\langle f \rangle = \frac{1}{N_p} \sum_{i=1}^{N_p} f_i \quad (3)$$

Assuming segregation direction of interest is defined by the unit vector $\vec{n}_s$ the segregation along this direction is hence characterised by a scalar value

$$S(t) = \vec{S}(t) \cdot \vec{n}_s \quad (4)$$

For a vertical case which is analysed in the present case, the direction of interest is along the gravity vector, therefore $\vec{n}_s = -\vec{g}/|\vec{g}|$ and the scalar equivalent of the parameter defined in Eq. (2) is

$$S(t) = \vec{S}(t) \cdot \frac{-\vec{g}}{|\vec{g}|} \quad (5)$$

Using this definition, $S(t) > 0$ if larger particles accumulate over the smaller ones (the "Brazilian nut" effect) and $S(t) < 0$ for the reverse "Brazilian nut" effect. Maximum possible value is $S = 1$, and minimum possible value is $S = -1$.

Finally, the segregation parameter S value of all simulated cases varies from -0.03 to 0.05 (Fig. 3), what corresponds to a nearly-uniform (unsegregated) state of the granular media. For cases including small particles, some segregation can be identified: smaller particles tend to collect on the bottom, and bigger particles - on the top, what can be additionally confirmed by view of the packed bed in Fig. 2 (a).

3.2. Porosity estimation

The volume of the simulation box was divided into test cells of size $\Delta_\varepsilon = 0.0005$ m for the case of $D_{min} = 1.76$ mm and $\Delta_\varepsilon = 0.001$ m for all other cases. $N_{shots} = 1000$ points (shots) were evenly distributed in each cell and tested on being inside of any particle or void space. The porosity of the cell having centre position (x,y,z) was defined as ratio of points N_{vs} being in void space with total number of points $N_{shots} = 1000$:

$$\varepsilon(x,y,z) = \frac{N_{vs}}{N_{shots}} \quad (6)$$

Finally, in order to avoid the influence of the packed bed top surface, box bottom and surrounding side walls on near wall porosity variation [9,49], mean core porosity ε was estimated in the core of the packed bed:
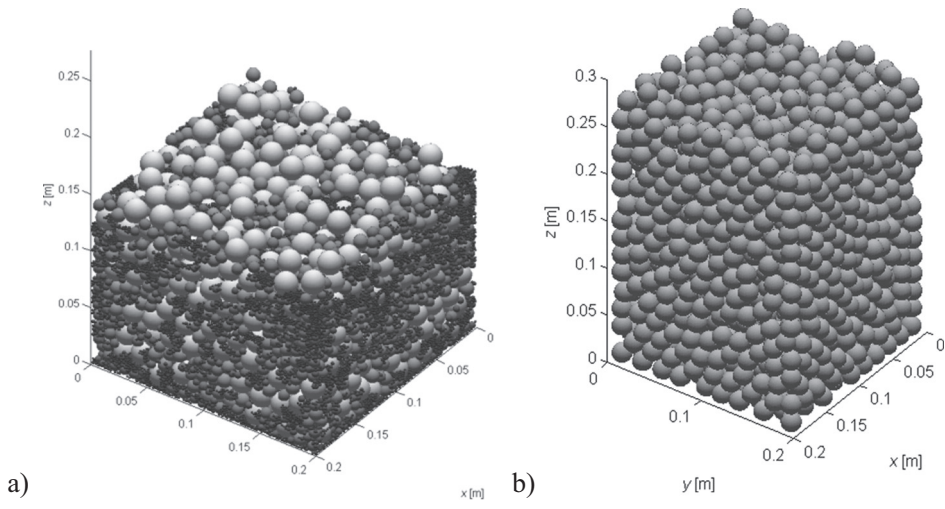
Table 2
Mechanical properties of the particle material.

Parameter	Notation	Value	Dimension
Diameter	D_f	1.76–18.24	mm
Density	ρ	500	kg/m³
Elastic modulus	E	100	MPa
Poisson modulus	σ	0.2	–
Normal dissipation coefficient	γ_n	100	1/s
Shear modulus	G	30	MPa
Shear dissipation coefficient	γ_t	100	1/s
Rolling resistance coefficient	k_{roll}	0	–
Dynamic friction coefficient	μ	0.8	–

Fig. 2. Packing of particles with different fractions: a) $D_{min} = 1.76$ mm ($N_p = 60,000$), b) $D_{min} = D_{max} = 18.24$ mm ($N_p = 2000$).

$$\varepsilon = \frac{1}{V_{core}} \int_{V_{core}} \varepsilon(x,y,z) dV \qquad (7)$$

where V_{core} is the volume of area inside the packed bed core defined in a distance $\Delta_{core} = 3 \cdot D_{max} = 55$ mm from the surrounding side walls and both the bottom and the top of the packed bed.

4. Results

Finally, the dependency of the wood chips packed bed, consisting of size fractions listed in Table 1, core porosity ε on size of smallest particles in a fraction D_{min} is depicted in Fig. 4. For each case of D_{min}/D_{max} several simulations with different particles number, and consequently with different particle total volumes, were simulated and resulting average value of the core porosity $\overline{\varepsilon}$ was calculated. The core porosity of the monodisperse packing of the packed bed containing only the biggest particles ($D_f = D_{min} = D_{max} = 18.24$ mm) is in range of 0.378 − 0.393 with average value $\overline{\varepsilon} = 0.389$, which is close to value 0.38 reported in [9,49].

As it was expected for the polydisperse case ($D_f \in [D_{min}, D_{max}]$, $D_{min} \in \{1.76, 2.81, 5.21, 6.90, 8.64, 10.52\} < D_{max} = 18.24$ mm), the core porosity decreases with decreasing D_{min} size of the smallest particle fraction, because smaller particles tend to fill up void space between bigger particles. For the case of the polydisperse packed bed consisting of size fractions up to the smallest simulated particle diameter $D_{min} = 1.76$ mm ($D_{min}/D_{max} = 0.096 \approx 0.1$), the core porosity has an approximate value of 0.28, which is less than the obtained value 0.33 for the Rosin-Rammler size distribution with the particle size ratios of $D_{min}/D_{max} = 0.1$ and 0.2 [9], because the particles pack denser in case of our particle size distribution.

Remarkably, the core porosity of the packed bed can be described by fractal law (Fig. 5):

$$\varepsilon\left(\frac{D_{min}}{D_{max}}\right) = a_\varepsilon + b_\varepsilon \cdot \left(\frac{D_{min}}{D_{max}}\right)^n \qquad (8)$$
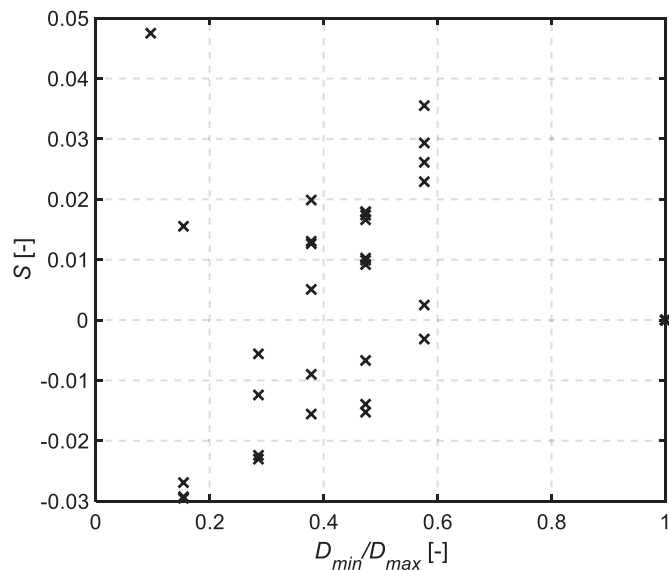

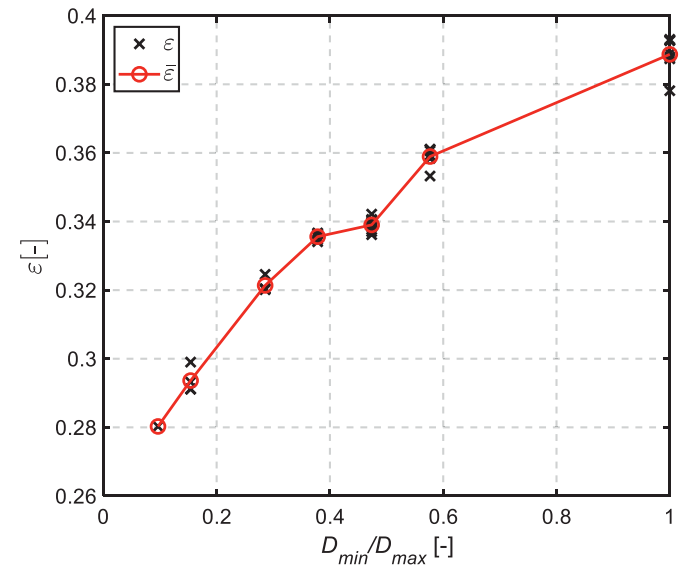**Fig. 3.** Particles size segregation S for all simulated cases.

Fig. 4. Dependency of the packed bed core porosity ε on size of smallest particles in fraction.
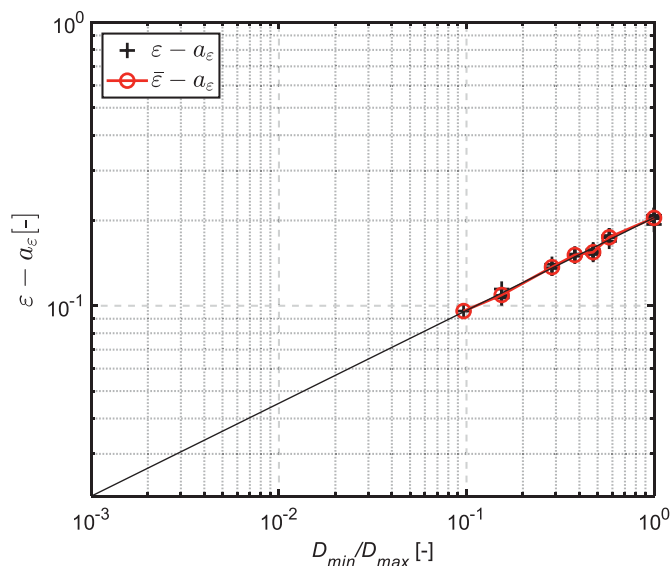
Fig. 5. Fractal dependency of the packed bed core porosity ε on size of smallest particles in fraction.

where n is a fractal dimension. The linear fitting of the simulated porosity, with standard deviation $\sigma = 0.00847$, gives the fractal dimension $n = 0.328$ and values for constants $a_\varepsilon = 0.185$ and $b_\varepsilon = 0.205$.

Consequently, if the law of porosity dependency on the smallest fraction size is known, the porosity for the packed bed containing smaller particles up to dust can be extrapolated as follows:

$$\lim_{D_{min} \to 0} \varepsilon \left(\frac{D_{min}}{D_{max}} \right) = a_\varepsilon = 0.185 \tag{9}$$

5. Conclusions

Number of particles is a limiting factor for DEM simulations, as the computational time increases with the number of particles. Therefore, the numerical simulation of packed beds with millions of particles is still not feasible. To overcome this issue, it is common to neglect small particles in the bed. However, due to missed small particles, the porosity of the packed is underestimated, what has an impact on fluid flow and consequently heat and mass transfer in the bed.

The present study demonstrates the dependency of the bed porosity on the smallest particle size in a packed bed. This relation allows us to extrapolate the bed porosity for a packed bed containing small particles up to dust without considering them in the computational domain of a coupled CFD-DEM model. Such approach significantly reduces the computational time of a CFD-DEM numerical modelling.

The results showed that the bed porosity decreases with decreasing the size of the smallest particle. Moreover, the core porosity of the bed was described by fractal law. The obtained relation is applicable only for a bed formed by spherical particles according to the size distribution of chosen wood chips. However, this study demonstrates the possibility to use the proposed approach for other types of granular materials.

CRediT authorship contribution statement

Algis Džiugys: Conceptualization, Software, Investigation, Methodology, Writing – original draft. **Amir Houshang Mahmoudi:** Conceptualization, Writing – original draft. **Edgaras Misiulis:** Data curation, Visualization, Writing – original draft. **Robertas Navakas:** Methodology. **Gediminas Skarbalius:** Data curation, Writing – review & editing.

References

[1] Musielak G. Modeling of heat and mass transfer during ultrasound-assisted drying of a packed bed consisting of highly shrinkable material. Chem Eng Res Des. 2018;129: 25–33. https://doi.org/10.1016/j.cherd.2017.10.031.

[2] Markovic M, Bramer EA, Brem G. Experimental investigation of wood combustion in a fixed bed with hot air. Waste Manag. 2014;34:49–62. https://doi.org/10.1016/j.wasman.2013.09.021.

[3] Jaberi H, Mosleh S, Dashtian K, Salehi Z. Fluid based cigarette carbonaceous hydrochar supported ZIF-8 MOF for CO2 capture process: the engineering parameters determination for the packed bed column design. Chem Eng Process Process Intensif. 2020;153:108001. https://doi.org/10.1016/j.cep.2020.108001.

[4] Stengler J, Linder M. Thermal energy storage combined with a temperature boost: an underestimated feature of thermochemical systems. Appl Energy. 2020;262:114530. https://doi.org/10.1016/j.apenergy.2020.114530.

[5] Anovitz LM, Cole DR. Characterization and analysis of porosity and pore structures. Rev Miner Geochem. 2015;80:61–164. https://doi.org/10.2138/rmg.2015.80.04.

[6] Sui L, Yu J, Cang D, Miao W, Wang H, Zhang J, Yin S, Chang K. The fractal description model of rock fracture networks characterization. Chaos Solitons Fractals. 2019;129: 71–6. https://doi.org/10.1016/j.chaos.2019.07.055.

[7] Li Z, Wan J, Huang K, Chang W, He Y. Effects of particle diameter on flow characteristics in sand columns. Int J Heat Mass Transf. 2017;104:533–6. https://doi.org/10.1016/j.ijheatmasstransfer.2016.08.085.

[8] Liu HB, Zhao CY. Effect of radial porosity oscillation on the thermal performance of packed bed latent heat storage. Engineering. 2021;7:515–25. https://doi.org/10.1016/j.eng.2020.05.020.

[9] Schulze S, Nikrityuk PA, Meyer B. Porosity distribution in monodisperse and polydisperse fixed beds and its impact on the fluid flow. Part Sci Technol. 2015;33:23–33. https://doi.org/10.1080/02726351.2014.923960.

[10] Gao P, Zhang TS, Wei JX, Yu QJ. Evaluation of RRSB distribution and lognormal distribution for describing the particle size distribution of graded cementitious materials. Powder Technol. 2018;331:137–45. https://doi.org/10.1016/j.powtec.2018.01.079.

[11] Rosin P. Laws governing the fineness of powdered coal. J Inst Fuel. 1933;7:29–36.

[12] Alderliesten M. Mean particle diameters. Part VII. The rosin-rammler size distribution: physical and mathematical properties and relationships to moment-ratio defined mean particle diameters. Part Part Syst Charact. 2013;30:244–57. https://doi.org/10.1002/ppsc.201200021.

[13] Vítěz T, Trávníček P. Particle size distribution of a waste sand from a waste water treatment plant with use of Rosin-Rammler and Gates–Gaudin–Schumann mathematical model. Acta Univ Agric Silvic Mendelianae Brun. 2011;59:197–202. https://doi.org/10.11118/actaun201159030197.

[14] Maćías-Garćía A, Cuerda-Correa EM. Application of the Rosin–Rammler and Gates–Gaudin–Schuhmann models to the particle size distribution analysis of agglomerated cork. Mater Charact. 2004;52:159–64. https://doi.org/10.1016/j.matchar.2004.04.007.

[15] Colorado-Arango L, Menéndez-Aguado JM, Osorio-Correa A. Particle size distribution models for metallurgical coke grinding products. Metals (Basel). 2021;11. https://doi.org/10.3390/met11081288.

[16] Bagnold RA, Barndorff-Nielsen O. The pattern of natural size distributions. Sedimentology. 1980;27:199–207. https://doi.org/10.1111/j.1365-3091.1980.tb01170.x.

[17] Fieller NRJ, Gilbertson DD, Olbricht W. A new method for environmental analysis of particle size distribution data from shoreline sediments. Nature. 1984;311:648–51.

[18] Guo Z, Sun Z, Zhang N, Cao X, Ding M. Mean porosity variations in packed bed of monosized spheres with small tube-to-particle diameter ratios. Powder Technol. 2019;354:842–53. https://doi.org/10.1016/j.powtec.2019.07.001.

[19] von Seckendorff J, Achterhold K, Pfeiffer F, Fischer R, Hinrichsen O. Experimental and numerical analysis of void structure in random packed beds of spheres. Powder Technol. 2021;380:613–28. https://doi.org/10.1016/j.powtec.2020.11.026.

[20] Ito D, Ito K, Saito Y, Aoyagi M, Matsuba K, Kamiyama K. Estimation of porosity and void fraction profiles in a packed bed of spheres using X-ray radiography. Nucl Eng Des. 2018;334:90–5. https://doi.org/10.1016/j.nucengdes.2018.05.003.

[21] Guo Z, Sun Z, Zhang N, Ding M, Cao X. Radial porosity peak at the centerline of packed beds with small tube to particle diameter ratios. Powder Technol. 2017; 319:445–51. https://doi.org/10.1016/j.powtec.2017.06.061.

[22] Zhang S, Liu W, Granata G. Effects of grain size gradation on the porosity of packed heap leach beds. Hydrometallurgy. 2018;179:238–44. https://doi.org/10.1016/j.hydromet.2018.06.014.

[23] Du W, Quan N, Lu P, Xu J, Wei W, Zhang L. Experimental and statistical analysis of the void size distribution and pressure drop validations in packed beds. Chem Eng Res Des. 2016;106:115–25. https://doi.org/10.1016/j.cherd.2015.11.023.

[24] Mueller GE. Radial void fraction distributions in randomly packed fixed beds of uniformly sized spheres in cylindrical containers. Powder Technol. 1992;72:269–75. https://doi.org/10.1016/0032-5910(92)80045-X.

[25] Balzan R, Sellerio AL, Mari D, Comment A. High-precision MRI reconstruction algorithm for 3D sphere packings. Appl Magn Reson. 2015;46:633–42. https://doi.org/10.1007/s00723-015-0677-0.

[26] Schneider FA, Rippin DWT. Determination of the local voidage distribution in random packed beds of complex geometry. Ind Eng Chem Res. 1988;27:1936–41. https://doi.org/10.1021/ie00082a030.

[27] Suikkanen H, Ritvanen J, Jalali P, Kyrki-Rajamäki R. Discrete element modelling of pebble packing in pebble bed reactors. Nucl Eng Des. 2014;273:24–32. https://doi.org/10.1016/j.nucengdes.2014.02.022.

[28] Yang X, Gui N, Tu J, Jiang S. 3D DEM simulation and analysis of void fraction distribution in a pebble bed high temperature reactor. Nucl Eng Des. 2014;270:404–11. https://doi.org/10.1016/j.nucengdes.2014.02.010.

[29] Navakas R, Džiugys A, Peters B. A community-detection based approach to identification of inhomogeneities in granular matter. Phys A Stat Mech Its Appl. 2014;407:312–31. https://doi.org/10.1016/j.physa.2014.04.003.

[30] Džiugys A, Peters B, Navakas R, Misiulis E. Density segregation on a moving grate. Powder Technol. 2017;305:323–32. https://doi.org/10.1016/j.powtec.2016.09.040.

[31] Zhu HP, Zhou ZY, Yang RY, Yu AB. Discrete particle simulation of particulate systems: theoretical developments. Chem Eng Sci. 2007;62:3378–96. https://doi.org/10.1016/j.ces.2006.12.089.

[32] Pozzetti G, Jasak H, Besseron X, Rousset A, Peters B. A parallel dual-grid multiscale approach to CFD–DEM couplings. J Comput Phys. 2019;378:708–22. https://doi.org/10.1016/j.jcp.2018.11.030.

[33] Buss F, Wirtz S, Scherer V. Simulation of a reacting agitated bed of straw pellets by a resolved coupled DEM/CFD method using a blocked-off approach. Int J Therm Sci. 2020;152:106332. https://doi.org/10.1016/j.ijthermalsci.2020.106332.

[34] Wang Z, Liu M. Semi-resolved CFD–DEM for thermal particulate flows with applications to fluidized beds. Int J Heat Mass Transf. 2020;159:120150. https://doi.org/10.1016/j.ijheatmasstransfer.2020.120150.

[35] Mohammad Mohseni B, Peters ADziugys. Applying XDEM to analyze the heat-up process of Woody biomass on a backward acting grate. J Energy Power Eng. 2017. https://doi.org/10.17265/1934-8975/2017.08.003.

[36] Mahmoudi AH, Hoffmann F, Peters B. Application of XDEM as a novel approach to predict drying of a packed bed. Int J Therm Sci. 2014;75:65–75. https://doi.org/10.1016/j.ijthermalsci.2013.07.016.

[37] Peters B, Džiugys A, Navakas R. Simulation of thermal conversion of solid fuel by the discrete particle method. Lith J Phys. 2011;51:91–105. https://doi.org/10.3952/lithjphys.51204.

[38] Džiugys A, Peters B. An approach to simulate the motion of spherical and non-spherical fuel particles in combustion chambers. Granul Matter. 2001;3:231–66. https://doi.org/10.1007/PL00010918.

[39] Peters B, Džiugys A, Navakas R. A shrinking model for combustion/gasification of char based on transport and reaction time scales. Mechanika. 2012;18:177–85. https://doi.org/10.5755/j01.mech.18.2.1564.

[40] Peters B, Hoffmann F. Iron ore reduction predicted by a discrete approach. Chem Eng J. 2016;304:692–702. https://doi.org/10.1016/j.cej.2016.06.116.

[41] Cui J, Hou Q, Shen Y. CFD-DEM study of coke combustion in the raceway cavity of an ironmaking blast furnace. Powder Technol. 2020;362:539–49. https://doi.org/10.1016/j.powtec.2019.12.012.

[42] Farivar F, Zhang H, Tian ZF, Gupte A. CFD-DEM -DDM model for spray coating process in a Wurster coater. J Pharm Sci. 2020;109:3678–89. https://doi.org/10.1016/j.xphs.2020.09.032.

[43] Mol J, Shahi M, Mahmoudi A. Numerical modeling of thermal storage performance of encapsulated pcm particles in an unstructured packed bed. Energies. 2020;13. https://doi.org/10.3390/en13236413.

[44] Malekjani N, Jafari SM. Simulation of food drying processes by computational fluid dynamics (CFD); recent advances and approaches. Trends Food Sci Technol. 2018;78:206–23. https://doi.org/10.1016/j.tifs.2018.06.006.

[45] Norton T, Tiwari B, Sun DW. Computational fluid dynamics in the design and analysis of thermal processes: a review of recent advances. Crit Rev Food Sci Nutr. 2013;53:251–75. https://doi.org/10.1080/10408398.2010.518256.

[46] Jamaleddine TJ, Ray MB. Application of computational fluid dynamics for simulation of drying processes: a review. Drying Technol. 2010;28:120–54. https://doi.org/10.1080/07373930903517458.

[47] Džiugys A, Navakas R. The role of friction in mixing and segregation of granular material. Granul Matter. 2009;11:403–16. https://doi.org/10.1007/s10035-009-0145-3.

[48] Vorotinskienė L. Parameters affecting biomass drying during combustion in moving grate furnaces. Energetika. 2019;65:74–84. https://doi.org/10.6001/energetika.v65i1.3976.

[49] De Klerk A. Voidage variation in packed beds at small column to particle diameter ratio. AIChE J. 2003;49:2022–9. https://doi.org/10.1002/aic.690490812.